



ALMA MATER STUDIORUM
UNIVERSITÀ DI BOLOGNA

ARCHIVIO ISTITUZIONALE
DELLA RICERCA

Alma Mater Studiorum Università di Bologna Archivio istituzionale della ricerca

Solar driven micro-ORC system assessment for residential application

This is the final peer-reviewed author's accepted manuscript (postprint) of the following publication:

Published Version:

Ancona, M.A., Bianchi, M., Branchini, L., De Pascale, A., Melino, F., Peretto, A., et al. (2022). Solar driven micro-ORC system assessment for residential application. RENEWABLE ENERGY, 195, 167-181 [10.1016/j.renene.2022.06.007].

Availability:

This version is available at: <https://hdl.handle.net/11585/894319> since: 2024-05-14

Published:

DOI: <http://doi.org/10.1016/j.renene.2022.06.007>

Terms of use:

Some rights reserved. The terms and conditions for the reuse of this version of the manuscript are specified in the publishing policy. For all terms of use and more information see the publisher's website.

This item was downloaded from IRIS Università di Bologna (<https://cris.unibo.it/>).
When citing, please refer to the published version.

(Article begins on next page)

Solar driven micro-ORC system assessment for residential application

Maria Alessandra Ancona, Michele Bianchi, Lisa Branchini, Andrea De Pascale, Francesco Melino, Antonio Peretto, Chiara Poletto*, Noemi Torricelli

*Alma Mater Studiorum – University of Bologna
Department of Industrial Engineering, Viale del Risorgimento 2, 40136 Bologna, Italy
E-mail address: chiara.poletto3@unibo.it*

ABSTRACT

The purpose of this study is to estimate the electricity production obtainable by coupling an existing kW-size recuperated Organic Rankine Cycle (ORC) prototype with a commercial solar thermal collector to reduce the yearly electricity purchased by a single-family user. A detailed semi-empirical steady-state model, validated against experimental data, is employed for the power plant simulation. The optimal sizes of both the collector surface and the storage tanks were assessed considering that a solar collector surface larger than 32.25 m² would lead the micro-ORC working in off-design conditions; while storage volumes higher than 6000 l become too large to be completely exploited.

Then, different low global warming potential fluids and blends were simulated for comparison with HFC-134a, the reference fluid for low-temperature ORC. Results show that the integrated system working with R134a can cover approximately 39% of the yearly electricity demand, corresponding to more than 1150 kWh. The replacement of R134a with the alternative fluids results in a penalization in the output electric power, related to thermodynamic properties such as density, liquid viscosity, and latent heat. Indeed, with R1234yf barely 16% (466 kWh) of the yearly electricity demand is covered; whilst the blend R513A allows to reach only 17.5% (525 kWh).

KEYWORDS

Micro-ORC; thermal solar; R134a; low-GWP fluids; semi-empirical model; residential application.

1. Introduction

During the last decades, the release of ever greater quantities of carbon dioxide has contributed to significantly increase the greenhouse effect and, consequently, temperatures and climate are being altered. Hence, the research for measures and solutions to reduce the amount of greenhouse gases released into the atmosphere is one of the main challenges of the current century [1].

In this context, the Organic Rankine Cycle (ORC) technology might play a pivotal role in the power generation from low-grade heat sources (i.e. below 300 °C): the technology may be used to produce electrical energy recovering waste heat from industrial processes, which would otherwise be dissipated. In addition, ORC systems may be a solution to exploit renewable low-temperature heat sources such as geothermal, concentrated solar thermal, and biomass combustion [2]. In particular, technology in the field of renewable energy is advancing quickly, in order to boost a deeper penetration of Renewable Energy Sources (RES) to allow the transition towards sustainable energy systems [3]. Moreover, according to Pereira et al. [4], ORC seems to be the most suitable and promising technology to be used in cogeneration plants in residential areas, the so-called Combined Heat and Power production (micro-CHP) system.

Quoilin et al., in their survey [5], have made an overview of the various ORC applications: such technology is consolidated to recover low-temperature waste heat, released by some industrial

Nomenclature		<i>Subscripts</i>	
A	Area [m ²]	amb	ambient
AU	Global heat exchange coefficient [W K ⁻¹]	c	condensation
c _p	Specific heat at constant pressure [J kg ⁻¹ K ⁻¹]	con	conversion
h	Specific enthalpy [J kg ⁻¹]	el	electric
I	Irradiation [W K ⁻¹]	ex	exhaust
L	Length [m]	H2O	water
ṁ	Mass flow rate [kg s ⁻¹]	in	inlet
N	Rotation speed [rpm]	out	outlet
Nu	Nusselt number [-]	pump	pump
p	Pressure [bar, Pa]	ref	reference
Q	Quality [-]	sat	saturation
Q̇	Thermal power [W]	tot	total
s	Specific entropy [J kg ⁻¹ K ⁻¹]	v	vaporization
SC	Subcooling [K, °C]	wf	working fluid
SH	Superheating [K, °C]		
T	Temperature [K, °C]		
U	Global heat exchange coefficient [W m ⁻¹ K ⁻¹]		
V	Volume [m ³]		
ṽ	Volume flow rate [L s ⁻¹]		
Ẃ	Power [W]		
α	Convective heat transfer coefficient [W m ⁻¹ K ⁻¹]		
Δ	Difference [-]		
ε	Heat exchanger efficiency [-]		
η	Efficiency [-]		
λ	Thermal conductivity [W m ⁻¹ K ⁻¹]		
μ	Dynamic viscosity [Pa s]		
ρ	Density [kg m ⁻³]		
		<i>Abbreviations</i>	
		CD	condenser
		COLL	collector
		EV	evaporator
		EXP	expander
		liq	liquid
		PP	pump
		REC	recuperator
		vap	vapour

43 processes, and to exploit geothermal sources, with the advantages of the programmability and the
44 continuity, and biomass, widely available in many agricultural and industrial processes.

45 ORC systems represent an interesting solution also to exploit solar radiation, by obtaining thermal
46 energy through solar collectors: Dickes et al. [6] analysed and reviewed some of the most interesting
47 and technologically innovative solutions of solar ORC. Solar thermal seems to be the most suitable
48 renewable energy source to be applied in residential areas [4][7], to which micro-generation
49 technologies (such as micro-ORC technology) are aimed. Solar thermal is characterized by: i) medium-
50 low temperatures (<130 °C), ii) high reliability, iii) ease of use and maintenance, iv) compact size and
51 v) the possibility of using different fluids for the heat exchange.

52 In solar applications, the main disadvantages are the non-programmability of the source and the
53 oscillation of its intensity. In this regard, Soulis et al. [8] found out that the solar radiation variation is
54 not only a function of the latitude but also of the altitude, as it affects the climate variability: this wide
55 spatial variability on the received solar radiation deeply influences the operation efficiency and the
56 produced power of an integrated system that includes solar collectors combined with an ORC engine.

57 The ORC technology is quite mature for medium and large size applications, while it is still at the
58 prototypal stage as far as micro-generation (plants not exceeding 15-20 kW) is concerned [9]. Since
59 plants of this size are particularly interesting in the residential sector, scientific research is aimed at
60 improving the performance of micro-ORC plants, both analyzing the influence of the working and
61 environmental conditions [10], and developing dynamic control strategies to deal with solar radiation
62 fluctuations.

63 Few studies have been conducted about solar thermal coupled with ORC technology. Lombardo et
64 al. [11] proposed a dynamic model of a small-sized trigeneration system intended for residential use: it
65 consists of a solar collector, the prototypal micro-ORC test rig considered in the current study, and an
66 absorption refrigeration system. In this study, the Authors highlight the promising features of ORC
67 technology in a trigeneration plant, which has an overall efficiency of 63%.

68 Calise et al. [12] presented a detailed techno-economic analysis of a prototypal small-scale solar
69 CHP system, based on the coupling of evacuated flat-plate solar thermal collectors with a small ORC.
70 The system results to be economically feasible for the majority of locations in the Mediterranean area.
71 Roumpedakis et al. [13] proposed the exergetic and economic performance assessment of a solar-driven
72 small-scale ORC for application in the South-East Mediterranean region, under multiple scenarios:
73 Authors carried out the analysis considering three collectors typologies working at a different
74 temperature, a wide range of working fluids and different installation sites.

75 Another interesting domestic scale solar-ORC system is proposed by Kutlu et al. [14], in which the
76 ORC is coupled with a vapour compression cycle (VCC) to work in three different modes: the ORC-
77 VCC system uses solar radiation to produce electric power and cooling in the summertime, power and
78 heating or just heating in the wintertime. Quoilin et al. in their work [15] presented an innovative
79 reversible energy conversion system for domestic application: the system can work either as an ORC
80 unit or a heat pump (HP), depending on the weather conditions (irradiation and ambient temperature)
81 and the heat required in the building.

82 Liu et al. [16] developed a dynamic fuzzy logic control strategy to maximize the solar radiation
83 absorption, increase the electric power output and improve the thermal efficiency: Authors modelled
84 their non-recuperative 1-kWe ORC test facility using Dymola software in Modelica environment and
85 virtually connected the model with the output thermal power of a solar field simulated in Simulink.

86 Furthermore, solar systems can easily be integrated into hybrid solutions in which different
87 renewable energy sources may compensate and overcome the drawbacks of the individual system. In
88 this regard, Ciani Bassetti et al. [17] proposed a detailed design and off-design model of a real hybrid
89 geothermal-solar power plant composed of a parabolic trough collector solar field and an air-cooled
90 binary cycle geothermal plant: they showed an increase in the system efficiency and the annual net
91 output power.

92 Another crucial aspect of the research in the ORC field is the selection of the working fluid,
93 affecting the system design and performance [18]. The selection of the working fluid for the ORC
94 technology is critical since the fluid must not only have thermophysical properties that match the
95 application, but also meet safety requirements and economic costs [19]. Since the great effect on the
96 system operation and energy efficiency, and since the impact on the environment, some procedures have
97 been developed to compare the performances of pure working fluids [20]. Tchanche et al. [21]
98 comparatively assessed the thermodynamic and environmental properties of a few fluids for small scale
99 solar applications.

100 More in detail, the most common fluids employed for low-temperature applications are refrigerants
101 belonging to HydroFluoroCarbons (HFCs) category [22][23]. Refrigerants seem to be very performing
102 for these applications thanks to their thermodynamic properties [24]: the low critical temperature allows
103 to exploit heat available at relatively low temperature, and the positive or null slope of the vapour
104 saturation limit curve allows to perform a dry expansion, even without superheating the working fluid.
105 One more advantage of refrigerants is related to the high density, which results in more compact system
106 layouts and components.

107 Critical issues related to HFCs are that they present a high Global Warming Potential (GWP),
108 meaning that, if released into the environment, they contribute to increase the amount of greenhouse
109 gases present in the atmosphere. Possible modern substitutes for HFCs have been identified in the
110 HydroFluoroOlefines (HFOs), which present similar properties to HFCs, but much lower GWP values.
111 A temporary solution to smooth the transition to HFOs working fluids lies in blends, made up of
112 hydrofluorocarbons and hydrofluoroolefines [25][26]. Molés et al. [27] carried out a comparison among
113 the predicted ORC performances of two low-GWP fluids (R1234yf and R1234ze) and R134a.
114 However, some studies reveal that low-GWP fluids could not always guarantee the same
115 performance as commonly used fluids [28]. Wang and Zhao [29] investigated the possibility of using
116 zeotropic mixtures instead of pure fluids for power generation in low-temperature solar Rankine cycles.
117 Abadi et al. [30] showed that a new zeotropic mixture of R245fa 60% / R134a 40% increases the power
118 output compared to an identical ORC with pure R245fa, despite working at a lower pressure ratio.

119 *1.1. Contribution of this paper*

120 Based on the above literature review, just a few studies have been published about the application
121 of the ORC technology to the solar thermal energy source for residential use. Furthermore, to the
122 Authors' knowledge, in current literature, there are no available works investigating the performance of
123 new generation fluids (HFOs) and their mixtures when used in solar applications at very low
124 temperatures. Thus, the purpose of this study is to enrich the present literature on this topic by comparing
125 the performance that might be reached, with low-GWP working fluids, by coupling an existing micro-
126 ORC prototype system with a commercial solar collector.

127 The Authors propose an extension of the detailed steady-state simulation model of the
128 aforementioned system, already developed and validated in previous works [22][31]. Overall estimation
129 of the annual energy production when it is applied to a residential building in the Italian town of Bologna
130 is performed. From historical data on solar radiation, it was possible to estimate the average irradiation
131 profile of each month and to evaluate the performance of the system at various times of the year. A
132 comparison was made among the performance of the system obtained by simulating its behaviour when
133 R134a, the fluid currently available in the plant, and five low-GWP alternatives (R1234yf, R1234ze(E),
134 R1243zf, R513A, R515A) are used as working fluids.

135 The first part of the article is dedicated to a brief description of the approach adopted to model the
136 system, highlighting the key features of each sub-model and the way they are linked together. Compared
137 to the previous Authors' studies, the solar collector and the hot water circuit models and regulation
138 strategy are integrated into the calculation code. The working fluid selection, since one of the most
139 critical design aspects in the ORC technology, is also discussed.

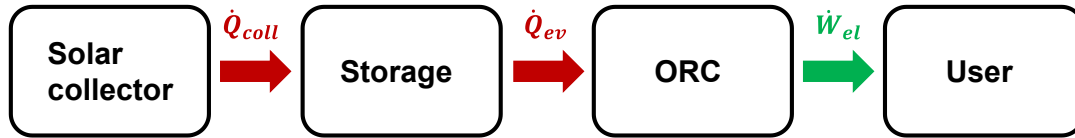
140 In the second part of the article, the Authors show and comment on the results of the simulations
141 performed by considering the average daily profiles of irradiation and ambient temperature for each
142 month in Bologna: a parametric analysis is carried out by varying the solar collector surface and the
143 storage dimensions to find the couple of parameters which maximize the output electricity production;
144 then a performance comparison is realized with different fluids and mixtures. The discussion is carried
145 out by comparing performance indexes and the annual electricity production obtained with the different
146 fluids.

147 **2. Material and Methods**

148 In this section, a detailed description of the approach adopted to model the system is given. First,
149 the system is described as a whole, and then a focus on each main component modelling is provided.
150 The section ends with an explanation of the fluid selection, and the description of the boundary
151 conditions and the regulation strategy adopted in the simulations.

152 2.1. Layout and model of the system

153 The modelled energy system consists of a micro-ORC conceived to supply electric power to a
154 single-family residential user. The system exploits solar radiation through an external circuit made up
155 of a commercial thermal solar collector and a thermal energy storage system (Figure 1).
156

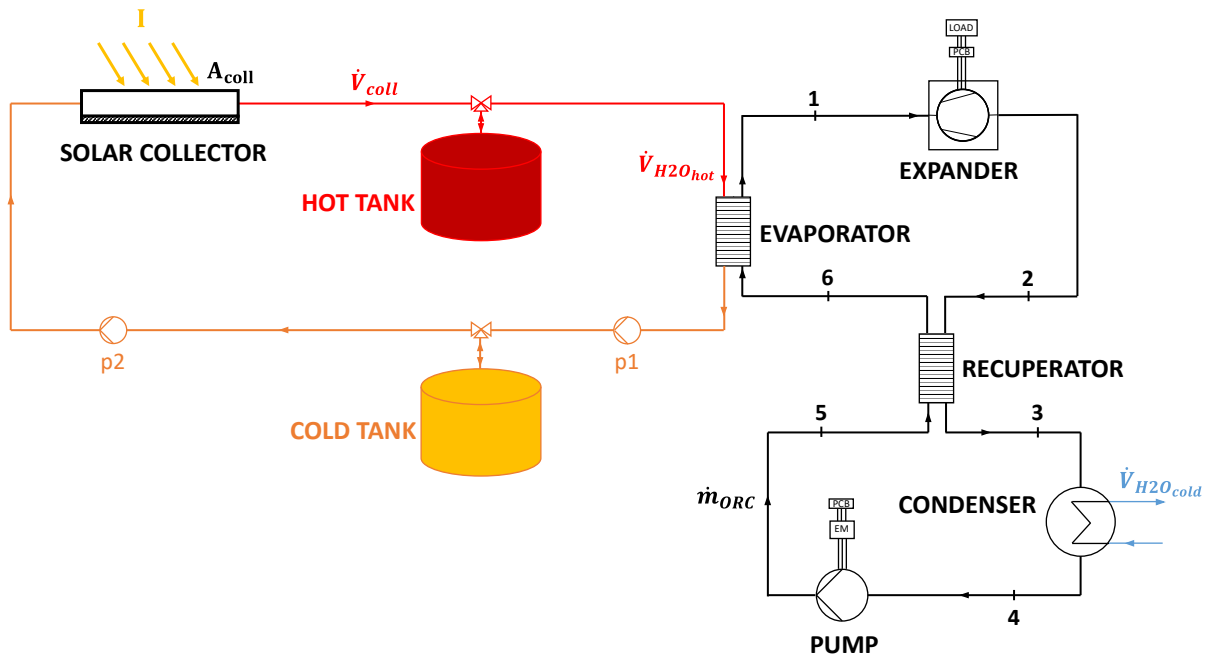


157
158 Figure 1. Conceptual scheme of the energy system with main thermal and electric power flows

159 A thermodynamic steady-state semi-empirical model of the system has been implemented to predict
160 the actual energy performance, under variable input from the solar source. More in detail, the modelled
161 system layout is shown in Figure 2 and described below. According to the scheme, the micro-ORC
162 model introduced in previous works of the Authors [31][22], has been coupled with a heat source circuit
163 model comprising: a flat plate thermal solar collector and two storage tanks, which decouple the solar
164 collector thermal power production from the ORC evaporator thermal demand, depending on the user
165 electricity demand.

166 The heat transfer fluid is water, which transfers thermal power from the collector to the storage
167 system, and from the storage to the organic working fluid at the ORC evaporator. The solar collector
168 has been sized to work at the nominal point under the reference case study operating conditions,
169 represented by 800 W/m² of irradiance and ambient temperature equal to 20 °C. To ensure the optimal
170 ORC operation, 2 °C of water temperature glide through the evaporator and 2 l/s of water flow rate (for
171 a thermal power of about 16 kW) are considered when sizing the solar collector under the
172 aforementioned boundary conditions.

173 Under these assumptions, a solar collector capturing surface equal to about 32.25 m² is chosen for
174 the case study (more details on the solar collector characteristics are provided in the dedicated paragraph
175 2.2). The storage tanks size is chosen equal to 6000 l, as a compromise between the desire of realising
176 the ORC operation from the solar radiation fluctuations and the need of limiting the overall dimensions,
177 as a potential residential application (see paragraph 4.2 for further details on the tanks and the solar
178 collector sizing).

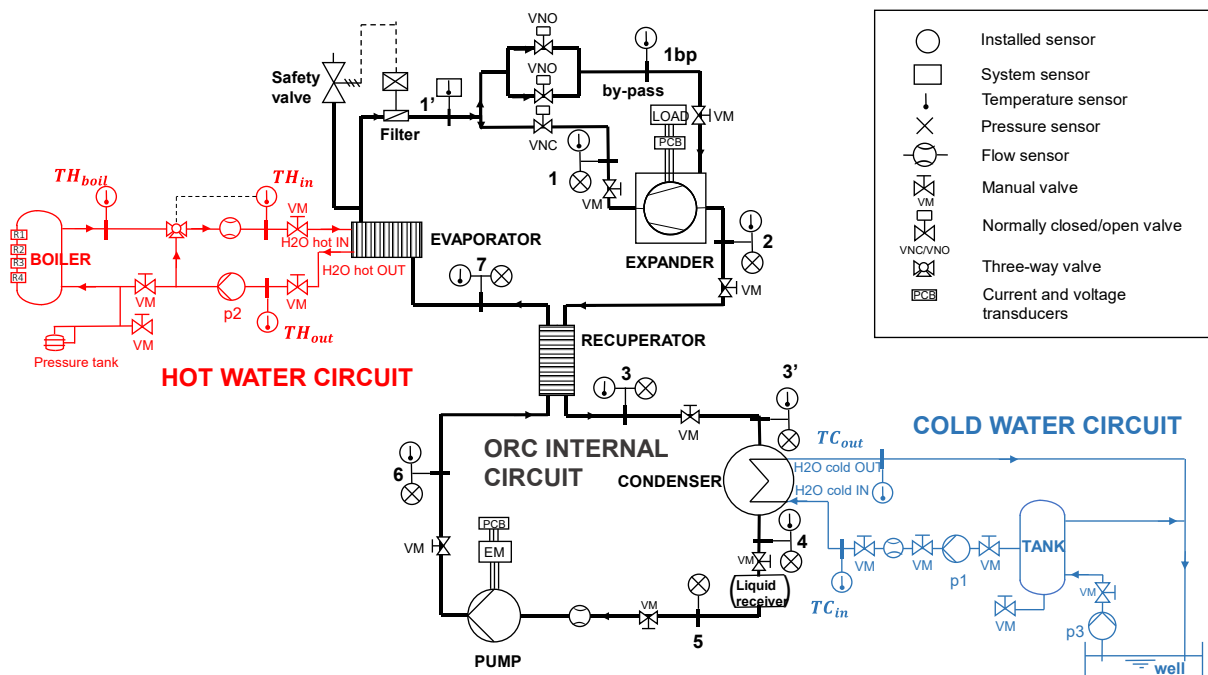


179

180

Figure 2. The integrated solar-ORC system layout

181



182

183

Figure 3. Micro-ORC test bench layout

184 The micro-ORC performance model is validated by taking as reference the small-scale prototype
 185 test rig (Figure 3) developed in the micro-generation laboratory of the University of Bologna [32]. The
 186 reference system consists of a kW-size recuperated micro-ORC, conceived for heat source temperature
 187 below 100 °C.

188 The key component of the system is the expander, a prototype of a reciprocating pistons model,
 189 directly coupled with the generator, which is connected to an electrical load, made of five pure resistive

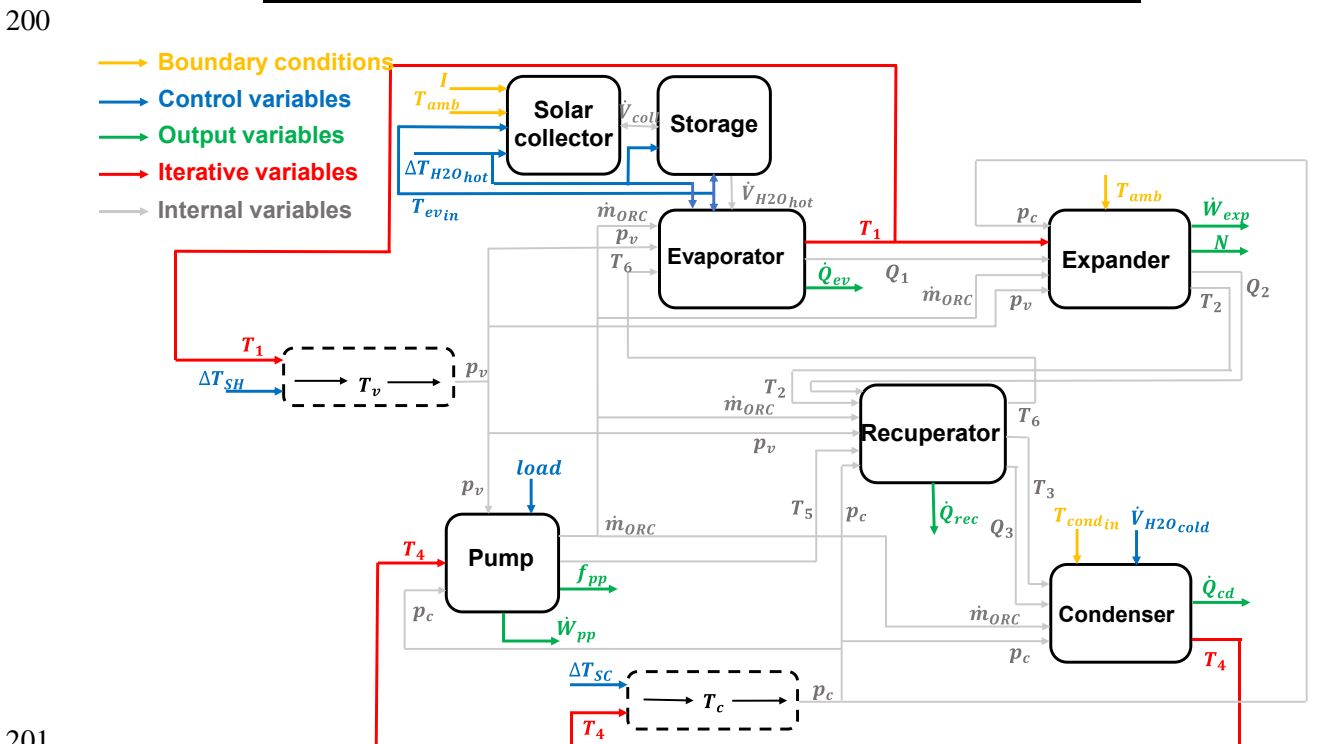
190 loads. The ORC feed pump is an external gear type, driven by an asynchronous electric motor, which is
 191 driven by a frequency inverter, allowing a proper regulation of the flow rate of the working fluid.

192 The heat exchangers are commercial brazed plate (evaporator and recuperator) and shell-and-tube
 193 (condenser) heat exchangers. The evaporator has been tested with hot water supplied by an electric
 194 heater of 40 kW nominal thermal power (high enough to cover the simulated operation in which the
 195 ORC input thermal power is around 16 kW); the condenser has been tested with cold water provided at
 196 variable ambient temperature by a well installed in the laboratory [31].

197 The operating ranges of key variables in which the micro-ORC prototype has been tested and the
 198 corresponding performance are reported in Table 1.

199 Table 1. Micro-ORC tested conditions and power ranges

ORC power output	0 – 1800 W
Hot water temperature	45 – 95 °C
Cold water temperature	14 – 28 °C
ORC mass flow rate	0.05 – 0.14 kg/s
R134a vaporization pressure	11 – 19 bar
R134a condensing pressure	5 – 8 bar



201 Figure 4. Model block diagram representing the main modelled components of the system and the
 202 interconnection variables
 203

204 Each component of the considered system has been modelled according to a semi-empirical
 205 approach with lumped parameters: rather than a constant-efficiency or a polynomial-based model, a

206 lumped parameters one is more accurate in simulating the performance of ORC systems, with robust
 207 prediction in both fitting and extrapolation [33].

208 The model has been implemented in MATLAB environment; the thermodynamic properties of the
 209 fluids have been calculated using REFPROP library [34].

210 Figure 4 shows a scheme of the system model, highlighting the components sub-models blocks and
 211 the involved thermodynamic variables. The components sub-models refer to: the expander; the ORC
 212 pump; the evaporator; the recuperator; the condenser; and the thermal solar collector. Each component
 213 is modelled as a MATLAB function and validated with experimental data collected during the reference
 214 rig experimental tests, using R134a as ORC working fluid [32]. The sub-models functions are linked
 215 together through the respective input and output variables, representing the thermodynamic conditions
 216 of the fluid at the inlet and outlet of the different components.

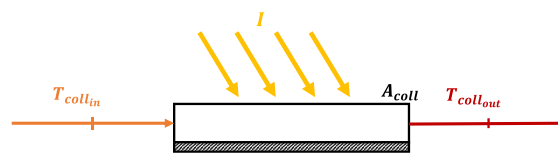
217 The inputs of the model are the boundary conditions of the system and the variables that can be
 218 controlled from the outside: the boundary conditions are the solar radiation (I), the ambient temperature
 219 (T_{amb}), and the cold source temperature ($T_{H2O_{cold}}$); whilst the control variables are the evaporator inlet
 220 temperature ($T_{ev_{in}}$), the hot water temperature difference between the inlet and the outlet of the
 221 evaporator ($\Delta T_{H2O_{hot}}$), the superheating level at the expander inlet (ΔT_{SH}), the electric load ($load$), the
 222 water volumetric flow rate at the condenser inlet ($\dot{V}_{H2O_{cold}}$), and the subcooling level at the condenser
 223 outlet (ΔT_{SC}).

224 Since the model is formulated as two levels implicit problem, its solution is determined through an
 225 iterative process with two iterative variables: the expander inlet temperature (T_1) and the condenser
 226 outlet temperature (T_4).

227 The output variables are the expander output power (\dot{W}_{exp}) and its shaft rotational speed (N), the
 228 pump absorbed power (\dot{W}_{pp}) and its frequency (f_{pp}), the thermal input provided at the evaporator (\dot{Q}_{ev}),
 229 the condenser discharged heat (\dot{Q}_{cd}), and the thermal power exchanged in the recuperator (\dot{Q}_{rec}).

230 2.2. Solar collector model

231 According to Garcia-Saez et al. [35], a 0-dimensional approach was adopted to model the flat solar
 232 collector behaviour in quasi-static equilibrium conditions. The thermal solar collector model reproduces
 233 the energy balance between the incident solar radiation (I) hitting the absorbing surface (A_{coll}), and the
 234 thermal power transferred to the water crossing the component (Figure 5).



235
 236 Figure 5. Scheme of the flat-plate thermal solar collector

237 Heat absorbed at the collector surface, \dot{Q}_{coll} , is evaluated through Eq. (1):

$$238 \quad \dot{Q}_{coll} = \eta_{coll} \cdot I \cdot A_{coll} \quad (1)$$

239 The collector efficiency, η_{coll} , is given by the following equation:
 240
 241

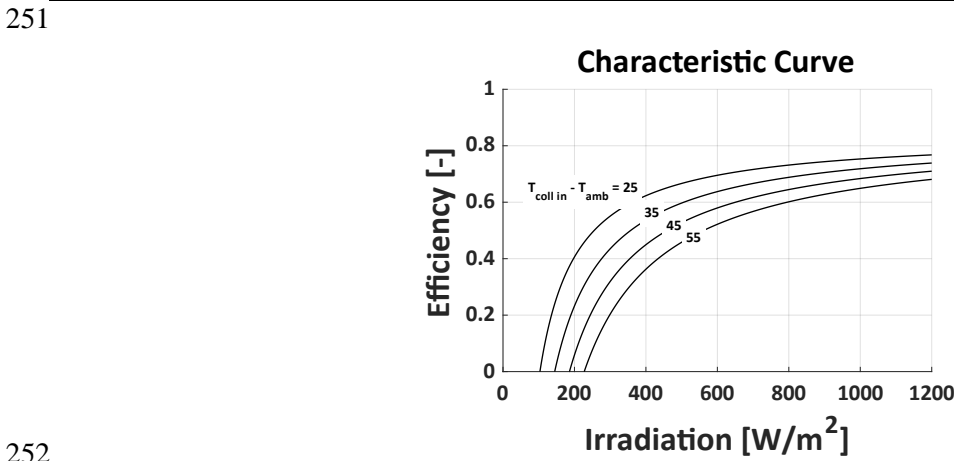
$$242 \quad \eta_{coll} = \eta_0 - a_1 \cdot \frac{T_{coll_{in}} - T_{amb}}{I} - a_2 \cdot \left(\frac{T_{coll_{in}} - T_{amb}}{I} \right)^2 \quad (2)$$

243 in which η_0 , a_1 and a_2 are parameters provided by the collector catalogue [36]; $T_{coll_{in}}$ is the water
 244 temperature at the solar collector inlet, which is equal to the water temperature at the evaporator outlet
 245 ($T_{ev_{out}}$); and T_{amb} is the ambient temperature.

246 Table 2 reports the solar collector's main specifications for a single panel, including the cited
 247 parameters. It can be noticed that the solar collector capturing surface size (equal to about 32.25 m²) is
 248 obtained by assembly of 15 panels of the chosen model. The solar collector characteristic curve, obtained
 249 from Eq. (2), is also shown in Figure 6.

250 Table 2. Thermal solar collector single panel specifications

Surface [m ²]		Absorber			Stagnation Temperature [°C]	Dimensions [mm]			Weight [kg]
Total	Absorbent	η_0	a_1 [W/(m ² K)]	a_2 [W/(m ² K ²)]		L	H	P	
2.57	2.15	0.839	3.47	0.0106	214	2077	1238	100	46



252 Figure 6. Thermal solar collector characteristic curves

254 The energy balance on the collector provides, as output, the water temperature value at the inlet of
 255 the evaporator, $T_{ev_{in}}$, which is equal to the water temperature at the outlet of the solar collector $T_{coll_{out}}$
 256 (Eq. (3)):

$$257 \quad T_{coll_{out}} = T_{coll_{in}} + \frac{\dot{Q}_{coll}}{\dot{V}_{H2O_{hot}} \cdot \rho_{H2O_{hot}} \cdot c_{p_{H2O_{hot}}}} \quad (3)$$

258 The effects of radiative losses, condensation, axial conduction and heat dissipation to the external
 259 environment have been neglected.

261 2.3. Storage model

262 The storage tanks are modelled as containers which are filled or emptied, according to the mass
 263 balance between the inlet and the outlet flow rate, depending on the solar collector and the evaporator
 264 operation.

265 In particular, when the water flow rate crossing the solar collector, \dot{V}_{coll} , is higher than the
 266 evaporator demanded flow rate, $\dot{V}_{H2O_{hot}}$, the hot tank is filled, and the cold tank is emptied of the same
 267 water volume; conversely, when the solar collector water flow rate decreases under the evaporator
 268 request, the hot tank turns to be emptied and the cold tank is filled. According to the balances presented

269 in Eq. (4) and Eq. (5), the water volume values inside the hot ($V_{hot_{tank_0}}$) and cold tank ($V_{cold_{tank_0}}$) are
 270 updated to their new values ($V_{hot_{tank}}$ and $V_{cold_{tank}}$) after the time $t_{filling/emptying}$:
 271

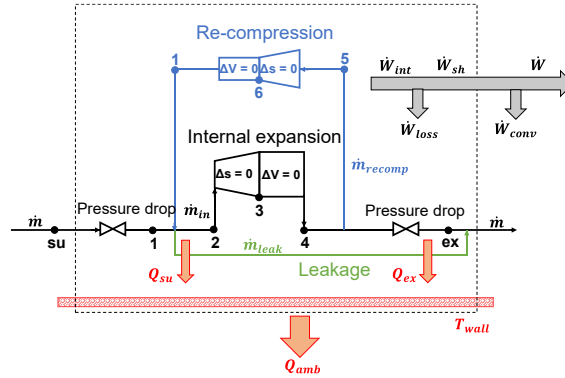
$$V_{hot_{tank}} = V_{hot_{tank_0}} + (\dot{V}_{coll} - \dot{V}_{H2O_{hot}}) \cdot t_{filling/emptying} \quad (4)$$

$$V_{cold_{tank}} = V_{cold_{tank_0}} + (\dot{V}_{H2O_{hot}} - \dot{V}_{coll}) \cdot t_{filling/emptying} \quad (5)$$

272
 273 A constraint is imposed to stop the filling (or emptying) when the tank is completely full (or empty).
 274 Thermal dissipation through the storage is considered negligible.

275 2.4. ORC reciprocating piston expander model

276 The volumetric piston expander is simulated through a grey-box model, validated for the reference
 277 reciprocating expander in a previous work of the Authors [37]. As an improvement of the model, in this
 278 study the possibility of simulating also a two-phase expansion was added. The model follows a lumped
 279 parameters approach as illustrated by the scheme shown in Figure 7.
 280



281
 282 Figure 7. Scheme of the expander model

283 The function models the cycle performed by the working fluid inside the expander to get the outlet
 284 thermodynamic conditions and the output electric power. It is based on equations describing the fluid
 285 admission, the internal expansion, the fluid exhaust, the re-compression phenomenon, and additional
 286 characteristic power losses.

287 The fluid admission and exhaust are modelled as the result of two stages each: the first stage is
 288 schematized as an isentropic flow through a converging nozzle (Eq. (6)), therefore only the pressure
 289 drop is considered; while in the second stage the pressure is assumed to remain constant and only the
 290 dissipation of thermal power is taken into account, according to the ε -NTU method (Eq. (7)):
 291

$$\dot{m}_{ORC} = \rho_{su/ex} \cdot A_{su/ex} \cdot \sqrt{2 \cdot |h_{su/ex} - h_{wf}|} \quad (6)$$

$$\dot{Q}_{su/ex} = \varepsilon_{su/ex} \cdot \dot{m}_{in} \cdot c_p \cdot (T_{wf} - T_{wall}) \quad (7)$$

292
 293 An equation similar to Eq. (6) is also used to estimate the leakage mass flow rate between the
 294 cylinder liner wall and the piston.

295 The internal expansion is schematized as the result of an isentropic expansion followed by a
 296 constant volume transformation, for which the isentropic expansion pressure ratio is determined by the
 297 built-in volume ratio parameter (see $r_{v_{exp}}$ in Table 3). In case the isentropic expansion ratio is different
 298 from the cycle expansion ratio, two different contributions of losses can affect the expander

299 performance, whether the pressure at the end of the isentropic transformation is higher or lower than the
 300 condensing one: namely the under-expansion or the over-expansion process.

301 The re-compression phenomenon (due to the presence of fluid trapped in the cylinder at the exhaust
 302 valve closure) is also modelled as an isentropic compression followed by a constant volume one,
 303 involving the mass flow rate, \dot{m}_{rec} .

304 Additional kinds of losses considered by the model are then the heat dissipation through the
 305 expander wall, the frictions, and the electro-mechanical conversion losses. Accounting for all these loss
 306 contributions, the output electric power is provided by Eq. (8):

$$307 \quad \dot{W}_{exp} = \left[\dot{m}_{in} \cdot (l_{exp_s} + l_{exp_v}) - \dot{m}_{rec} \cdot (l_{comp_s} + l_{comp_v}) - \dot{W}_{loss} \right] \cdot \eta_{con} \quad (8)$$

308 For a detailed description of the expander model please refer to the previous works of the Authors
 309 [31][37]. The input and output variables and the calibrated coefficient of the expander model are
 310 reported in Table 3.
 311

312 Table 3. Expander model parameters

Input		Calibrated Parameters		Output
\dot{m}_{ORC}	$AU_{su_{ref}}$	Supply heat transfer coefficient [W/K]	5.65e+05	\dot{W}_{exp}
T_1 or Q_1	$AU_{ex_{ref}}$	Exhaust heat transfer coefficient [W/K]	9.23e+05	T_2
p_1	AU_{amb}	Ambient heat transfer coefficient [W/K]	0.96	N
p_2	$r_{v_{exp}}$	Built-in volume ratio [-]	1.459	
T_{amb}	$r_{v_{comp}}$	Re-compression volume ratio [-]	1.25	
	V_0	Clearance volume [m ³]	2.32e-08	
	A_{leak}	Equivalent leakage area [m ²]	5.51e-06	
	A_{su}	Supply nozzle equivalent section [m ²]	1.75e-05	
	$\dot{W}_{loss_{ref}}$	Constant friction losses [W]	0.198	
	\dot{W}_{loss_N}	Proportional friction losses [W/min]	1.07e-05	

313
 314 **2.5. ORC pump and circuit resistance model**

315 According to the approach already proposed by the Authors [22][31], the pump function provides
 316 the operating point of the machine by crossing the resistance curve of the circuit (Eq. (10)) with the
 317 characteristic curve of the pump (Eq. (9)).

318 The resistance curve depends on the load, *load*, as the increase in the expander resisting load results
 319 in an increase in the resisting load on the whole circuit, and on the fluid density, ρ . The characteristic
 320 curve of the pump changes instead with its rotational speed, N_{pp} and the fluid dynamic viscosity, μ .
 321 Both the pump and the resistance characteristics can be expressed through the relationship between the
 322 pump pressure rise, Δp , and the elaborated volume flow rate, \dot{V} :

$$323 \quad \Delta p = (c_1 \cdot N_{pp} + c_2 \cdot \dot{V}) \cdot \mu \quad (9)$$

$$\Delta p = (c_3 \cdot load + c_4) \cdot \dot{V} \cdot \rho \quad (10)$$

324
325
326

Extrapolated curves of the gear pump under exam are shown in Figure 8 in terms of pressure rise versus volumetric flow rate. Calibrated coefficients are listed in Table 4.

Table 4. Pump model parameters

$V_{cc} [m^3]$	$6.2327e - 05$
$c_1 = \frac{c_2 \cdot V_{cc}}{60} [-]$	529.4055
$c_2 [m^{-3}]$	$5.0964e + 08$
$c_3 \left[\frac{Pa \cdot s}{kg} \right]$	1.5177
$c_4 \left[\frac{Pa \cdot s}{kg} \right]$	53.304

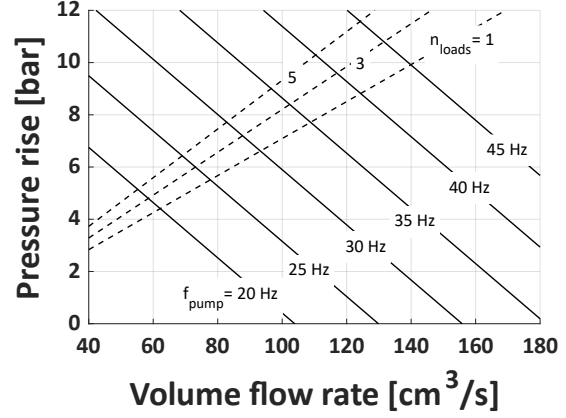


Figure 8. Pump characteristic and circuit resistance

327 2.6. ORC heat exchangers model

328 The three heat exchangers (evaporator, recuperator and condenser) are modelled employing a
329 lumped parameters moving boundary approach [38]. Each heat exchanger is decomposed into a number
330 of zones equal to the number of states experienced by the fluid inside the component [39]: in each zone,
331 and for its entire length, the fluid does not change phase. According to this approach, each zone is
332 characterized by a global heat exchange coefficient U_i and a heat transfer surface area A_i through which
333 a certain heat transfer process occurs [40].

334 The "moving-boundary" approach is particularly accurate as it allows to consider the great
335 variations of the global heat exchange coefficient occurring at the fluid changing phase. The boundaries
336 between consecutive zones are not fixed, but they move depending on the physical state of the fluid.
337 The only constraint is that their sum must be equal to the geometric surface of the component that is a
338 model parameter.

339 The evaporator and the condenser are modelled as decomposed into three zones (subcooled, two-
340 phase and superheated) each, while in the recuperator a single heat exchange zone is considered. The
341 heat transfer process occurring in the i -th zone is obtained using the ε -NTU (*Number of Transfer Units*)
342 method, according to the following three equations:
343

$$\dot{Q}_i = \varepsilon_i \cdot \dot{m}_{hot} \cdot c_{p_{hot_i}} \cdot (T_{in_{hot_i}} - T_{in_{cold_i}}) \quad (11)$$

$$\varepsilon_i = \frac{1 - e^{-NTU_i \cdot (1 - C_i^*)}}{1 - C_i^* \cdot e^{-NTU_i \cdot (1 - C_i^*)}} \quad (12)$$

$$NTU_i = \frac{U_i A_i}{C_{min_i}} \quad (13)$$

344
345

in which C_i^* is the ratio between the minimum and the maximum thermal capacity.

346 In the subcooling and the superheating zones, the considered global heat transfer coefficient
 347 accounts for the convective coefficient of the working fluid side (α_{wf_i}) and the convective coefficient
 348 of the water side (α_{H2O}), Eq. (14):
 349

$$U_i = \left(\frac{1}{\alpha_{wf_i}} + \frac{1}{\alpha_{H2O}} \right)^{-1} \quad (14)$$

350
 351 The water convective coefficients and the working fluid convective coefficients in the subcooling
 352 and superheating zones are evaluated through Dittus-Boelter correlation for forced convection. Instead,
 353 in the two-phase zone and the unique zone of the recuperator, the global heat transfer coefficient derives
 354 from empirical correlations. In particular, correlations used for the evaporator and the condenser have
 355 the form of Eq. (15), while the one used for the recuperator has the form of Eq. (16):
 356

$$U_{ev/cd} = U_{ev/cd_ref} \cdot \dot{m}^a \cdot \Delta T_{sat}^b \cdot \dot{m}_{H2O}^c \cdot p_{sat}^d \cdot \Delta h_{sat}^e \quad (15)$$

$$U_{rec} = U_{rec_ref} \cdot \dot{m}^a \cdot \Delta T^b \quad (16)$$

357
 358 In both the above equations the referencing heat transfer coefficients, $U_{ev/cd/rec_ref}$, and all the
 359 exponents have been numerically calibrated to fit the available experimental data. Eq. (15) takes into
 360 account the working fluid and water mass flow rates (\dot{m} and \dot{m}_{H2O}), the vaporization/condensation
 361 pressure (p_{sat}), the temperature difference between the water temperature and the saturation temperature
 362 of the working fluid (ΔT_{sat}), and the specific latent heat (Δh_{sat}). Eq. (16) considers just the working
 363 fluid mass flow rate (\dot{m}) and the inlet temperature difference of the two fluid streams (ΔT). Results of
 364 the numerical calibration are reported in Table 5.

365 Table 5. Heat exchangers models calibrated coefficients

Coefficients	Evaporator	Condenser	Recuperator
$U_{ev_ref} [W/(m \cdot K)]$	0.4046	0.0015	3.7914
$a [-]$	0.9153	0.8894	0.4636
$b [-]$	-0.9607	-0.8284	-0.0186
$c [-]$	-0.0214	-0.0014	
$d [-]$	0.1881	-0.0024	
$e [-]$	1.2056	1.9046	

366

367 2.7. Correction of fluid dependent parameters

368 Even though the majority of the empirical parameters requiring calibration are associated with the
 369 components' geometry, some depend on the working fluid thermodynamic characteristics. Indeed,
 370 global heat transfer coefficients are working-fluid dependent parameters that have to be corrected to
 371 account for the use of fluids different from R134a. For this reason, the global heat transfer coefficients
 372 are re-determined by adopting the procedure proposed by Giuffrida [41], when considering different
 373 fluids. Since the global heat transfer coefficient is defined as:
 374

$$AU = \frac{Nu \cdot \lambda}{L} \quad (17)$$

375
376
377
378
379

where Nu is the Nusselt number, λ is the conductivity and L is the characteristic length. The global heat transfer coefficient for the new fluid, AU_{fluid} , can be determined as function of the reference global heat transfer coefficient, AU_{R134a} , and the fluids properties, by Eq. (18):

$$\frac{AU_{fluid}}{AU_{R134a}} = \frac{Nu_{fluid} \cdot \lambda_{fluid}}{Nu_{R134a} \cdot \lambda_{R134a}} \quad (18)$$

380

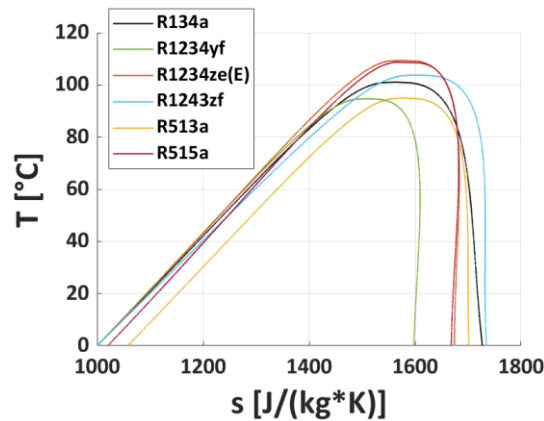
381 2.8. Fluid selection

382
383
384
385
386
387

In order to investigate in this micro-ORC application low-GWP working fluids [25][26] as alternatives to the basic R134a (GWP=1300 [42]), a comparison of different fluids has been performed. The alternative working fluids selected in this study in line with the current state-of-the-art of low-GWP refrigerants are three different hydrofluoroolefines, namely R1234yf (GWP<1), R1234ze(E) (GWP<1) and R1243zf (GWP<1 [43]), R513A (GWP=573), which is a mixture of 56% R1234yf and 44% R134a, and R515A (GWP=400), which is a mixture of 88% R1234ze(E) and 12% R227.

388
389
390
391
392
393
394
395

Very similar thermodynamic properties characterize the aforementioned fluids, namely saturation limit curves in the T-s diagram (Figure 9), critical temperature and pressure, density, viscosity, and latent heat. However, there are small differences that affect the performance of the system: in particular, density and viscosity affect losses due to leakages, and the heat transfer coefficient affects the dissipation of thermal power towards the environment. Table 6 shows density (ρ), viscosity (μ) and latent heat (Δh_{lat}) of each of the considered fluids at typical condensing and evaporating temperature values, respectively related to the ambient temperature and the source temperature.



396
397

Figure 9. Temperature-entropy diagram comparison of the considered micro-ORC fluids

398
399

Table 6. Working fluids thermodynamic properties on saturated curves at typical condensing and evaporating temperatures

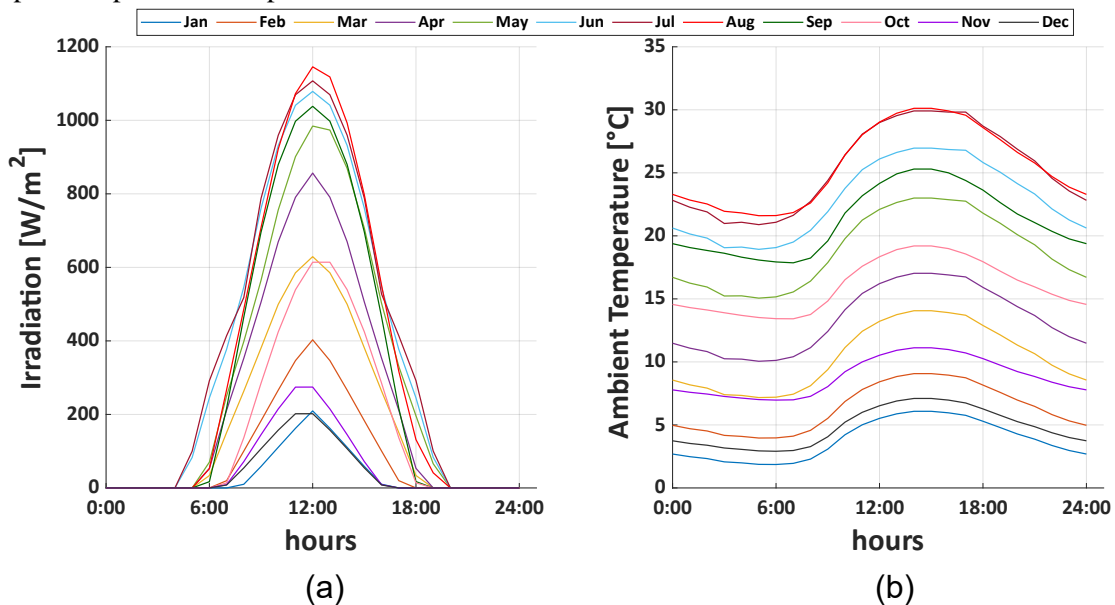
	ρ (T=18 °C) [kg/m ³]		ρ (T=65 °C) [kg/m ³]		μ (T=18 °C) [Pa·s·10 ⁴]		μ (T=65 °C) [Pa·s·10 ⁴]		Δh_{lat} (T=18 °C) [kJ/kg]	Δh_{lat} (T=65 °C) [kJ/kg]
	sat. liq.	sat. vap.	sat. liq.	sat. vap.	sat. liq.	sat. vap.	sat. liq.	sat. vap.		
R134a	1233	26.1	1026	100	2.13	0.114	1.15	0.140	184	132
R1234yf	1117	30.9	914	115	1.66	0.111	0.899	0.141	151	104
R1234ze(E)	1186	21.2	1010	80.1	2.08	0.118	1.15	0.148	172	130
R1243zf	999	21.9	837	78.8	1.71	0.111	0.981	0.136	187	138
R513A	1160	30.6	949	116	1.81	0.113	0.966	0.142	162	112
R515A	1210	21.9	1030	82.9	2.12	0.118	1.17	0.147	165	124

400

401 *2.9. Boundary conditions*

402 In order to estimate the yearly electric energy produced by the considered system, simulations were
 403 performed using the monthly averages of the daily hourly profiles of solar radiation. The adopted
 404 profiles are based on historical data for the city of Bologna (latitude around 44.5°N), and are provided
 405 by UNI 10349 standards [44] for July and September: these profiles are related to solar panels inclined
 406 by 30° (in Italy the electricity production is maximized with a tilt angle value between 30° and 35°,
 407 depending on the installation location), and south oriented in Bologna.

408 Normally, solar thermal panels are mounted with an inclination equal to the latitude increased by
 409 15° or 20° to maximize the production of hot water during the winter months [45]. However, since in
 410 this case the hot water is used to produce electricity, it is preferable to have an inclination that maximizes
 411 its production throughout the year: therefore, it is preferable to adopt the inclination that is normally
 412 adopted for photovoltaic panels.



413

414 Figure 10. Monthly-averaged Irradiation (a) and Ambient temperature (b) daily profiles

415 The monthly-averaged daily hourly profile was estimated for all the months of the year (Figure 10a)
 416 using the available profiles of July and September, and the monthly average values of daily solar
 417 radiation, by ENEA [46]. The corresponding monthly average profiles of the daily hourly ambient
 418 temperature are shown in Figure 10b. Then, the ORC performance was simulated with the model on
 419 each representative day of the month, assuming the input variables listed in Table 7.

420 Table 7. Input boundary conditions and control variables

Variable	Value					
$load$	3000 W					
T_{condin}	18 °C					
$\dot{V}_{H_2O_{cold}}$	2.77 L/s					
ΔT_{SC}	0.5 °C					
T_{evin}	53 - 65 °C					
$\Delta T_{H_2O_{hot}}$	2 °C					
ΔT_{SH}	R134a	R1234yf	R1234ze(E)	R1243zf	R513A	R515A
	3°C	15°C	10°C	10°C	20°C	10°C

421
 422 The ORC regulation strategy is conceived to maximize the ORC system's global efficiency during
 423 each operating hour with variable input thermal power from the renewable source. It must be highlighted
 424 that the superheating degree at the inlet of the expander is kept constant during the monthly simulations,
 425 but it varies according to the chosen fluid, to maximize the electric power output. The evaporator water
 426 temperature glide is kept constant and always equal to 2°C, whilst the evaporator water inlet temperature
 427 is kept fixed throughout the month, but it takes a different value each month depending on the average
 428 monthly irradiance.

429 The system performance and the electricity production are calculated on an hourly basis, according
 430 to a compromise between the need to appreciate the daily and yearly variability, and the need to keep
 431 low computational costs. Indeed, hourly data allow to detect the daily solar radiation (and the electric
 432 power output) trend without exponentially increasing the computational time and cost. Furthermore, the
 433 available irradiation and ambient temperature data are monthly averages, so a narrower discretization
 434 would not increase the accuracy of the simulated electricity production. Observing Figure 10, the hourly
 435 discretization allows to appreciate daily variations, and the monthly averages are sufficient to appreciate
 436 yearly variations.

437 2.10. Hot water flow rates regulation strategy

438 The water flow rate through the solar collector is regulated according to the solar radiation, whilst
 439 the evaporator water flow rate is attempted to be kept as close as possible to the reference conditions (2
 440 l/s), within the limits of the storage tanks capacity. Both the water flow rates through the solar collector
 441 and the evaporator are regulated by a control system which takes into account the value of the current
 442 solar radiation and the degree of filling of the storage tanks.

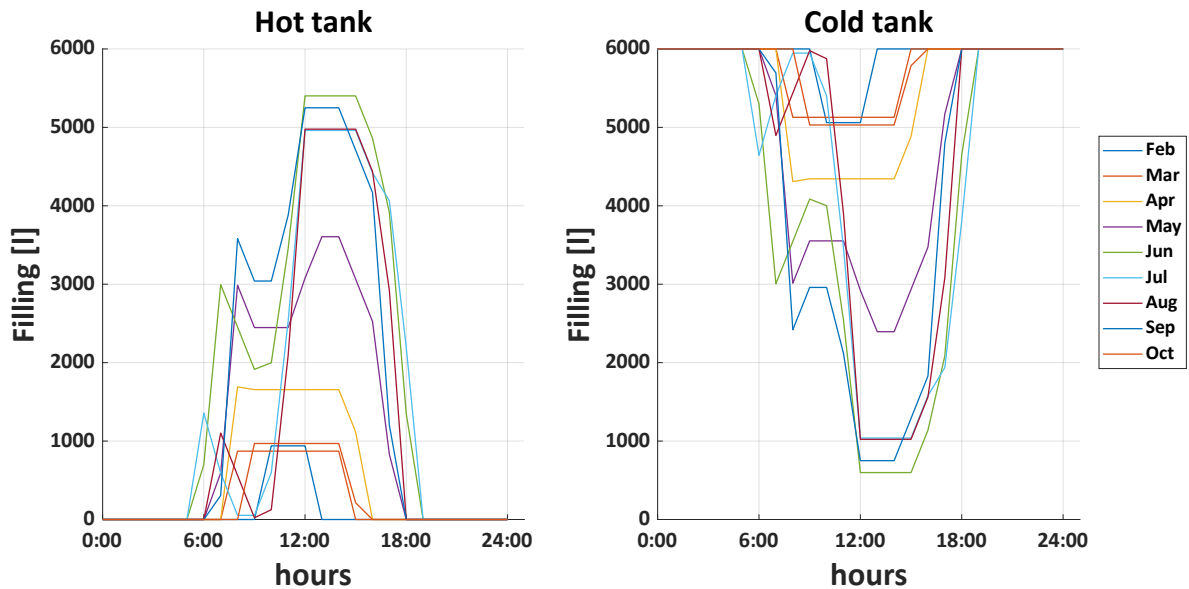
443 More in detail, first of all, the hot water control system checks if the irradiance value is null or not:
 444 - In case the solar radiation is absent, the control system checks if the hot storage tank is empty
 445 or not: if it is empty, no water flow rates are set up; otherwise, a water flow rate of 1.0 l/s
 446 (reference value) is set up in the loop crossing the evaporator, until the hot tank is not emptied.
 447 - In case the solar radiation is present, the control system regulates the hot water flow rate crossing
 448 the solar collector in such a way as to keep a glide of 2°C. The water flow rate through the
 449 evaporator follows the water flow rate through the collector for values higher than 0.4 l/s and

450 lower than 2.0 l/s. If the water flow rate through the collector is lower than 0.4 l/s, the ORC is
 451 kept off or works with a water flow rate higher than 0.4 l/s, depending on the grade of filling of
 452 the storage. If the water flow rate through the collector is higher than 2.0 l/s, the ORC works
 453 with a water flow rate of 2.0 l/s and the hot tank is filled.

454 To summarize, the control system tries to keep the ORC operation as close as possible to the
 455 reference operating condition to maximize the ORC efficiency. In case the solar irradiance overcomes
 456 the reference value of 800 W/m², the thermal power transferred to water across the solar collector is
 457 higher than the reference value (16 kW) exchanged in the evaporator: this means that the solar collector
 458 flow rate is higher than the evaporator flow rate, so the energy surplus is collected into the hot storage
 459 tank. On the contrary, when the solar radiation is lower than 800 W/m² or null, the evaporator demands
 460 a water flow rate greater than the one crossing the collector: so, the hot tank is emptied to satisfy the
 461 request, and the water surplus at the outlet of the evaporator is stored in the cold tank.

462 Figure 11 shows the filling and emptying of the storage tanks resulting in a variable state of charge
 463 throughout the day. In the first hours of the day, with rising thermal power from the sun but low
 464 irradiation intensity, the ORC system is kept off and the heated water is entirely collected inside the hot
 465 tank (while the cold tank is being emptied). The ORC is switched on when the minimum ORC output
 466 power conditions are reached; the hot tank continues to be filled during the central hours of the day, and
 467 eventually, it is emptied during the afternoon and the evening.

468



469

470

Figure 11. Daily profile of the storage tanks state of charge

471 3. Results and Discussion

472 In this section, first, the performance indexes used to show and discuss the results of the analysis
 473 are introduced. Then, a parametric analysis follows, to assess the optimal size of the solar collector
 474 capturing surface, and to observe the influence of the storage tanks' size on the performance. Eventually,
 475 the results of the simulated operation with the different working fluids are shown and discussed, using
 476 the performance indexes previously mentioned.

477 3.1. Performance indexes

478 Performance indexes, used to compare the different analysed configurations, are listed in Table 8;
 479 in particular the expander electric output power (\dot{W}_{exp}), the pump electric consumption (\dot{W}_{pp}), the net
 480 output power (\dot{W}_{net}), the back work ratio (BWR), the ORC efficiency (η_{tot}) are considered. Eventually,

481 the electricity production (E_{el}) is calculated as the hourly net output power (\dot{W}_{net}) multiplied by the
 482 ORC operation hours (t_{on}): both monthly and yearly values of the electricity production have been
 483 calculated.

484

Table 8. Performance indexes

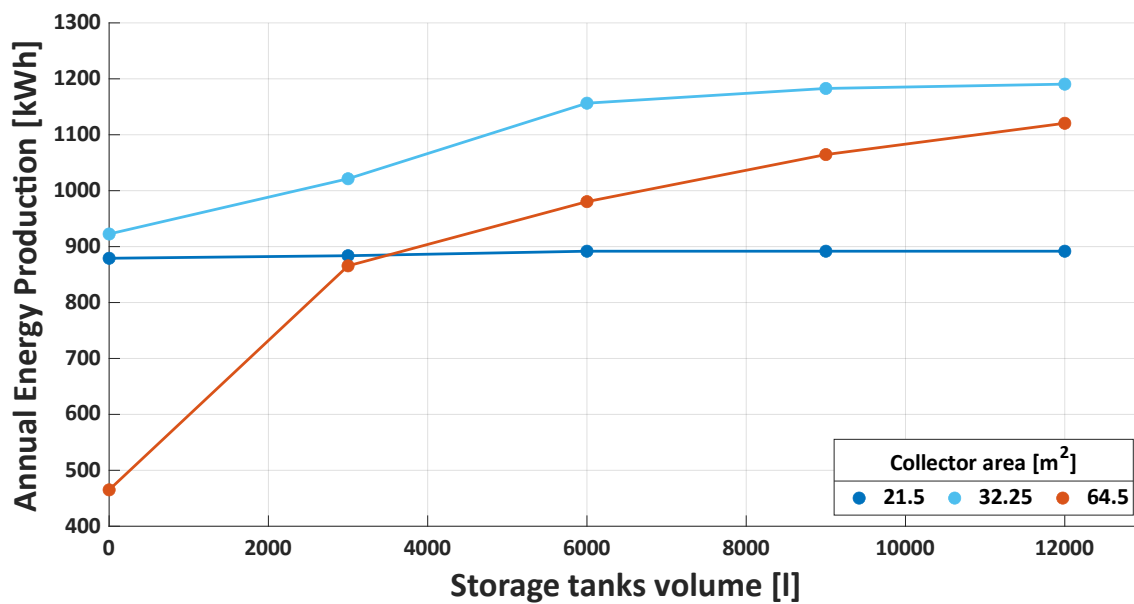
Expander Output Power	\dot{W}_{exp}
ORC Pump Consumption	\dot{W}_{pp}
Net Output Power	$\dot{W}_{net} = \dot{W}_{exp} - \dot{W}_{pp}$
Back Work Ratio	$BWR = \frac{\dot{W}_{pp}}{\dot{W}_{exp}}$
ORC Efficiency	$\eta_{tot} = \frac{\dot{W}_{exp} - \dot{W}_{pp}}{\dot{Q}_{ev}}$
Electricity Production	$E_{el} = \sum \dot{W}_{net} \cdot t_{on}$

485

486 *3.2. Parametric analysis: storage tanks and solar collector sizes*

487 A parametric analysis has been carried out to assess the optimal size of the solar collector capturing
 488 surface, and to investigate the change in the performance when varying the size of the hot storage tanks,
 489 for a given micro-ORC system size.

490 In the first instance, a reference solar collector area of 32.25 m² (corresponding to 15 panels of the
 491 adopted model) was selected. To verify that both smaller and larger capturing surfaces would decrease
 492 the electricity production of the system, simulations were performed also for the solar collector area
 493 equal to 21.5 m² (10 panels) and 64.5 m² (30 panels). Furthermore, the storage tanks volume was varied
 494 from 0 to 12000 l with a step of 3000 l to investigate the influence of the tanks size on the performance.



495

496 Figure 12. Yearly electricity production when varying the storage tank volume and the collector capturing
 497 surface

498 Figure 12 shows the simulated yearly electric energy produced by the system under the same
499 boundary conditions (Table 7) and with the reference working fluid (R134a), with the different
500 considered storage tanks volume and collector capturing surface values.

501 The increase of the hot storage tanks volume allows to progressively decouple the ORC loop
502 operation from the hot circuit conditions: as a consequence, it results in a beneficial effect on the ORC
503 performance and the electricity production. Indeed, when the irradiance is higher than the design value
504 (i.e., 800 W/m² for the reference case), the buffer receives the thermal power surplus, which is released
505 when the irradiation is lower. In this way, the optimal ORC boundary conditions, in terms of evaporator
506 water inlet temperature, are provided for as long as possible.

507 Moreover, Figure 12 highlights that the annual electricity production is almost independent of the
508 storage tanks volume when the collector area is small (21.5 m²). In this case, generally, the thermal
509 power input does not reach the reference value of 16 kW, so the available heat from the collector is
510 directly sent to the evaporator, and the storage thermal inertia is scarcely exploited (except when the
511 irradiance is very low). Among the simulated size values of the solar collector, a capturing surface of
512 32.25 m² is proved to be the solution which grants the highest production. Nevertheless, also in this case,
513 the electricity production approaches an asymptotic value because the storage capacity becomes too
514 large to be completely exploited. A storage volume of about 6000 l thus proved to be a good compromise
515 between dimensions and performance.

516 Further enlarging the solar collector surface (64.5 m²), under the assumption of keeping constant
517 the water temperature glide, the water flow rate increases to accommodate the available thermal power
518 input increase. However, due to the limited storage size, it becomes impossible to completely decouple
519 the hot circuit and the ORC operation: as a consequence, the organic fluid mass flow rate must also be
520 increased to face the thermal power input increase. Under these boundary conditions, the ORC is forced
521 to work in off-design conditions, with a derating of the system performance (mainly due to the increase
522 of the expander under-expansion losses and the pump consumption increase at the same time). In the
523 view of the above, the penalization of the electric energy production is more significant with a smaller
524 storage volume, due to the reduction in the storage thermal inertia.

525 It must be highlighted that the results of the collector size parametric analysis are specific for the
526 case study of a kW-size ORC; coupling a larger collector surface with a larger ORC would lead instead
527 to an increment in the electricity production. However, in this case, the dimensions would be no more
528 compatible with the residential application.

529 3.3. Working fluids performance comparison

530 Results of the fluid assessment show that the expander electric power output is greater when using
531 R134a as working fluid (Figure 13), since this fluid exhibits the highest isentropic enthalpy drop
532 available to the expansion process. Indeed, R134a has a higher liquid density and viscosity than those
533 presented by the other five fluids (Table 6), therefore it undergoes a lower pressure drop through the
534 expander inlet valve. By using R134a, it is possible to obtain an average expander power output higher
535 than 1000 W during the months between April and October, while with the low-GWP fluids it is not
536 higher than about 600 W.

537 During the winter months (November, December and January), solar radiation never reaches a
538 sufficient intensity to be exploited to produce electric energy.

539 Concerning the pump performance, R134a is the fluid with the maximum liquid viscosity (2.06 x 10⁻⁴
540 Pa·s) and thus the minimum leakage losses at the pump meatus affecting volumetric flow. In addition,
541 pump consumption is inversely proportional to the fluid density (Eq. (19)) (higher for R134a):
542

$$543 \dot{W}_{pp} = \frac{\dot{m}_{ORC} \cdot \Delta p}{\rho \cdot \eta} \quad (19)$$

544 However, pump consumption is higher in the case of the use of R134a (Figure 14), because a higher
 545 working fluid mass flow rate (Figure 15) is required since the imposed superheating degree is lower.

546 As a result, the system net power output is significantly higher when the plant behaviour is operated
 547 with R134a (Figure 16): values up to 500 W are reached, while with the low-GWP fluids values lower
 548 than 300 W occur all the year.
 549

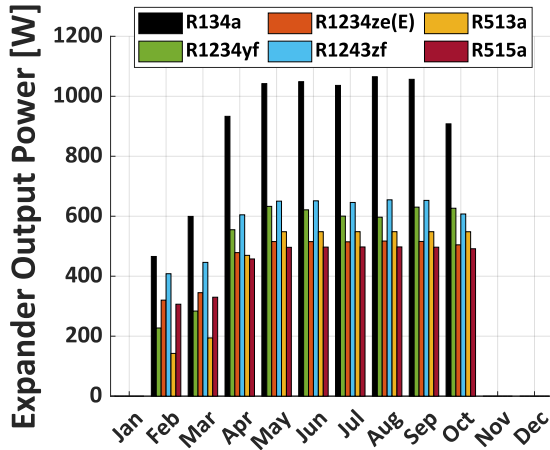


Figure 13. Monthly average expander output power

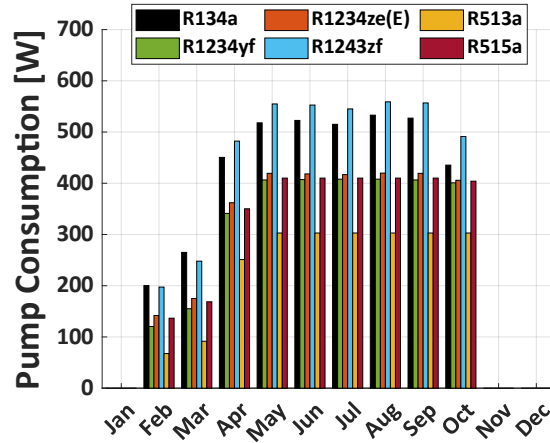


Figure 14. Monthly average pump consumption

550 Regarding the BWR (Figure 17), it reaches quite high values (always higher than 40%) with all the
 551 analyzed fluids due to the significant pump consumption, in line with typical values for ORC systems.

552 The highest efficiency (Figure 18) is reached with R134a (more than 2%). It must be highlighted
 553 that the analyzed system was properly designed to work with R134a and probably, redesigning the
 554 system for a new fluid would partially improve the overall performance when the new fluid is used.
 555 Nevertheless, it should be noticed that, considering the operating temperature levels of the sources of
 556 this application, the corresponding theoretical Carnot efficiency of the ORC system is lower than 14%.
 557

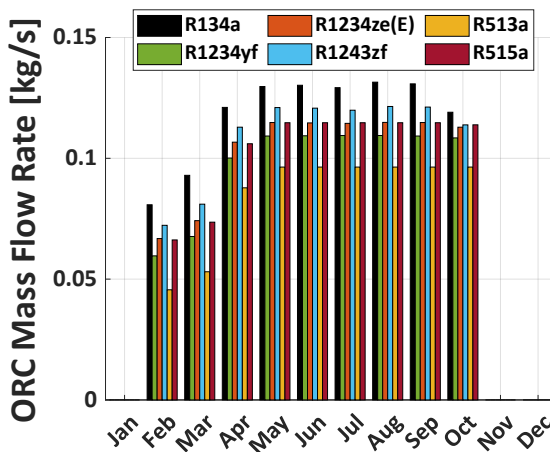


Figure 15. Monthly average ORC mass flow rate

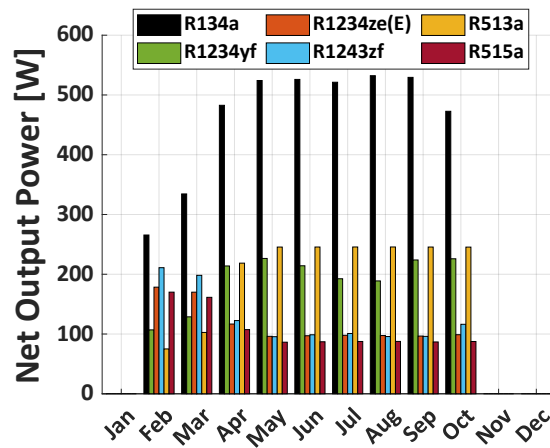


Figure 16. Monthly average net output power

558

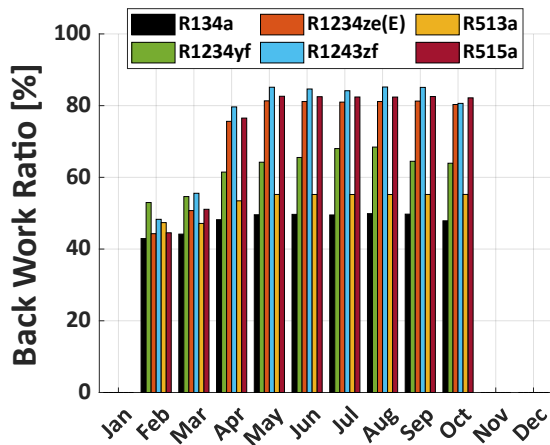


Figure 17. Monthly average back work ratio

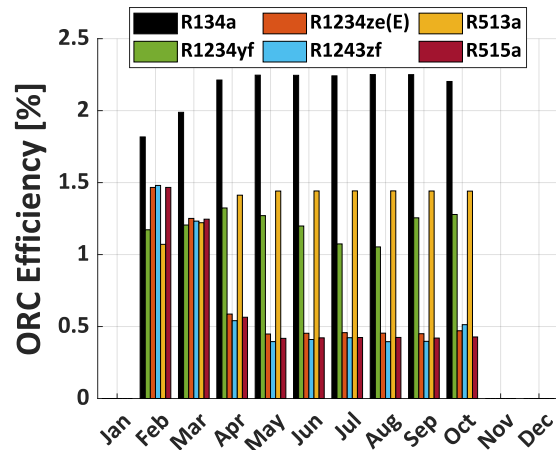


Figure 18. Monthly average ORC efficiency

559 Figure 19 shows the estimated monthly energy produced by the system. Annual electricity
 560 production of 1156.44 kWh is calculated, using R134a as working fluid; this energy production is about
 561 30% more than the value estimated in the same solar radiation and ambient temperature conditions, and
 562 with the same micro-ORC power plant, but without including the hot water storage tanks (equal to
 563 878.64 kWh per year, see Figure 12).

564 Considering a single-family user consumption value equal to 2996 kWh per year [47], the system
 565 would guarantee about 39% of the user demand (reduced to 29% in the case without thermal storage).
 566 According to the average price of electricity that occurred in Italy in 2019 (24.21 c€/kWh [48]), there
 567 would be an annual saving of € 280.

568 The reference micro-ORC test bench considered in this study is still a prototype not significant for
 569 the investment cost estimation. In order to estimate an approximate price of the whole simulated system
 570 (comprising the micro-ORC generator, the solar collector and the storage tanks), a market survey on
 571 similar systems has been carried out using web information and commercial components costs. In
 572 particular, regarding the ORC technology in the kW-size range, large uncertainties in cost estimation
 573 occur, because this is not very established on the market. According to the commercial information
 574 available from Air Square [49], the cost of micro-ORC systems can be estimated at approximately \$
 575 10,000 per installed kW. Considering an average conversion efficiency from euro to dollar [50], and
 576 estimating the storage tanks and the solar collector cost respectively 6,000 € and 4,000 € [51], the
 577 complete simulated system would cost about 17,000-19,000 €.

578 Thus the simulated system is still not competitive on the market, because it would have a pay-back
 579 period of more than 60 years, which is above the typically assumed system lifespan [52]. However, if it
 580 were possible to improve the efficiency of the system and increase the output power, it would be possible
 581 to save enough to allow a return on the initial investment in a few years.

582 An alternative solution consists in modifying the hot water circuit and increasing the solar radiation
 583 capturing surface to integrate the electric power with a thermal power production: an interesting layout,
 584 which could be investigated, would include the possibility of tapping hot water for a thermal user from
 585 the storage tanks. The hot circuit would be reintegrated upstream of the thermal solar collector with cold
 586 water, and the flow rate through it would be regulated in such a way as to guarantee the desired
 587 temperature at the inlet of the evaporator. Furthermore, by also including thermal production, it would
 588 be possible to turn off the ORC sub-system at lower solar radiation (and conversion efficiencies), but to
 589 exploit the system to satisfy a thermal request.

590 By using low-GWP fluids, the yearly electric energy production and the savings are lower: results
 591 are summarized in Table 9.

592 The performance comparison carried out in the current analysis emphasizes that, although there is
 593 an environmental benefit in terms of GWP, there is a penalty in terms of energy production when

594 conventional HFCs are replaced with alternative fluids. In the light of these results, it is evident that the
 595 research for fluids with a low environmental impact, which, at the same time, can ensure acceptable
 596 performance, is still fully open. However, the deep awareness of the causes of the low performance,
 597 obtained with low environmental impact working fluids, encourages further investigations.
 598

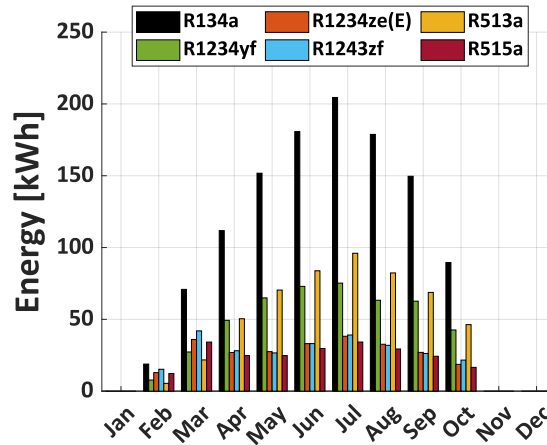


Figure 19. Output electric energy

599
600

Table 9. Estimated annual energy production

Working fluid	Electricity [kWh/year]	% of the satisfied requirement
R134a	1156.44	39.0%
R1234yf	466.01	16.0%
R1234ze(E)	252.92	8.0%
R1243zf	263.97	8.8%
R513A	525.21	17.5%
R515A	230.11	7.7%

601

602 4. Conclusions

603 A detailed semi-empirical steady-state simulation model of a kW-size micro-ORC prototypal
 604 system coupled with a commercial solar thermal collector is proposed. A performance comparative
 605 analysis on the estimated yearly electricity production for residential target with low-GWP working
 606 fluids to replace HFC-134a is provided.

607 The analysis was conducted on the reference small-scale test rig developed in the micro-generation
 608 laboratory of the University of Bologna (UNIBO-ORC test bench).

609 Semi-empirical models of all the main components, developed in the MATLAB environment, are
 610 detailed: the volumetric piston expander is simulated following a lumped parameters approach and
 611 validated for the reference reciprocating piston expander; the pump model provides the operating point
 612 of the machine by crossing the resistance curve of the circuit with the characteristic curve of the pump;
 613 the heat exchangers are modelled according to a lumped parameters moving boundary approach; the
 614 solar collector follows a 0-dimensional approach, which reproduces the energy balance between the
 615 incident solar radiation hitting the absorbing surface and the thermal power transferred to the hot water
 616 which supplies heat to the evaporator; a system of two storage tanks is included in the hot water circuit
 617 which feeds the evaporator.

618 Simulations were carried out considering a typical daily hourly profile of irradiation and ambient
619 temperature (for the Italian town of Bologna) for each month: these profiles are obtained as monthly
620 averages based on historical data. The system operation is evaluated at variable storage tanks size and
621 solar collector area, identifying the couple of parameters that maximize the generated electric energy.

622 Then, the performances of the system are simulated by comparing its behaviour when the currently
623 available working fluid, R134a, is replaced with five alternative low-GWP fluids: R1234yf,
624 R1234ze(E), R1243zf and the blends R513A and R515A. Results highlight that the net power output
625 produced with the low-GWP fluids is always lower than the one obtained with R134a (over 500 W)
626 because of both a smaller isentropic enthalpy drop available in the expander and relatively higher pump
627 consumption (due to the lower density of low-GWP fluids compared to R134a). Consequently, the BWR
628 reaches higher values when the low-GWP fluids are used, while the highest global efficiency (more than
629 2%) is achieved with R134a.

630 It must be pointed out that an accurate micro-ORC system redesign and optimization would
631 guarantee achieving higher components and overall performance with the alternative fluids analyzed.
632 The yearly electricity production with R134a is estimated to be higher than 1150 kWh, fulfilling
633 approximately 39% of the annual electric energy average single-family user requirement. Although the
634 performed comparison might discourage the use of low-GWP fluids to replace HFC-134a, the urgency
635 of the problems related to greenhouse gases emissions should push the research towards solutions which
636 can increase the performance of both HFOs and blends, as they may effectively help to reduce the
637 greenhouse gases impact.

638 Results could be extended including a deep and detailed economic analysis, providing a rigorous
639 estimation of costs and return on the investment. Moreover, an optimization of the performance of the
640 machines could be carried out, in order to include further results describing performance achievable
641 based on state-of-art machines efficiencies.

642 Furthermore, the possibility to add thermal power production could be investigated too in the future.
643 The analysis could be obtained by increasing the solar collector capturing surface and redesigning the
644 system regulation strategy: in this way, it would be possible to satisfy a thermal demand, especially at
645 lower solar radiation, when conversion efficiencies do not make the ORC convenient to use. Thus, the
646 development of all the above-mentioned investigations represents a possible future extension of the
647 current study.

648 **CRediT roles**

649 Maria Alessandra Ancona: supervision and investigation; Michele Bianchi: visualization and
650 project administration; Lisa Branchini: conceptualization and formal analysis; Andrea De Pascale:
651 funding acquisition, supervision and investigation, methodology, visualization; Francesco Melino:
652 resources and conceptualization; Antonio Peretto: funding acquisition; Chiara Poletto: software,
653 methodology, writing-original draft; Noemi Torricelli: data curation, methodology, writing-review and
654 editing.

655 **Acknowledgements**

656 The Authors thank the 16th Conference on Sustainable Development of Energy Water and
657 Environmental Systems - SDEWES, October 2021, Dubrovnik.

658 **Funding sources**

659 This research did not receive any specific grant from funding agencies in the public, commercial, or
660 not-for-profit sectors.

661 **References**

- 662 [1] P.A. Østergaard, N. Duic, Y. Noorollahi, S. Kalogirou, Latest progress in Sustainable
663 Development using renewable energy technology, *Renew. Energy*. 162 (2020) 1554–1562.
664 <https://doi.org/10.1016/J.RENENE.2020.09.124>.
- 665 [2] B.S. Park, M. Usman, M. Imran, A. Pesyridis, Review of Organic Rankine Cycle experimental
666 data trends, *Energy Convers. Manag.* 173 (2018) 679–691.
667 <https://doi.org/10.1016/j.enconman.2018.07.097>.
- 668 [3] P.A. Østergaard, N. Duic, Y. Noorollahi, S.A. Kalogirou, Recent advances in renewable energy
669 technology for the energy transition, *Renew. Energy*. 179 (2021) 877–884.
670 <https://doi.org/10.1016/J.RENENE.2021.07.111>.
- 671 [4] J.S. Pereira, J.B. Ribeiro, R. Mendes, G.C. Vaz, J.C. André, ORC based micro-cogeneration
672 systems for residential application - A state of the art review and current challenges, *Renew.*
673 *Sustain. Energy Rev.* 92 (2018) 728–743. <https://doi.org/10.1016/j.rser.2018.04.039>.
- 674 [5] S. Quoilin, M. Van Den Broek, S. Declaye, P. Dewallef, V. Lemort, Techno-economic survey
675 of Organic Rankine Cycle (ORC) systems, *Renew. Sustain. Energy Rev.* 22 (2013) 168–186.
676 <https://doi.org/10.1016/j.rser.2013.01.028>.
- 677 [6] Rémi Dickes, A. Desideri, E. Casati, S. Quoilin, From 1885 to nowadays: a (short) techno-
678 historical review of Solar Organic Rankine Cycle system, (2021) 1–8.
- 679 [7] P.A. Østergaard, N. Duic, Y. Noorollahi, H. Mikulcic, S. Kalogirou, Sustainable development
680 using renewable energy technology, *Renew. Energy*. 146 (2020) 2430–2437.
681 <https://doi.org/10.1016/J.RENENE.2019.08.094>.
- 682 [8] K. Soulis, D. Manolakos, E. Ntavou, G. Kosmadakis, R. Ike, T.P. Lefkippos, Preliminary
683 operation assessment of a two-stage ORC engine combined with evacuated tube solar collectors
684 throughout Greece, (2021) 1–9.
- 685 [9] Lorenzo Tocci, Tamas Pal, Ioannis Pasmazoglou, Benjamin Franchetti, Small Scale Organic
686 Rankine Cycle (ORC): A Techno-Economic Review, *Energies*. (2017).
- 687 [10] S. Quoilin, M. Orosz, H. Hemond, V. Lemort, Performance and design optimization of a low-
688 cost solar organic Rankine cycle for remote power generation, *Sol. Energy*. 85 (2011) 955–966.
689 <https://doi.org/10.1016/j.solener.2011.02.010>.
- 690 [11] W. Lombardo, S. Ottaviano, L. Branchini, S. Vasta, A. De Pascale, A. Sapienza, A dynamic
691 model of a solar driven trigeneration system based on micro-ORC and adsorption chiller
692 prototypes, in: *AIP Conf. Proc.*, American Institute of Physics Inc., 2019: p. 020098.
693 <https://doi.org/10.1063/1.5138831>.
- 694 [12] F. Calise, M.D. D’Accadia, M. Vicidomini, M. Scarpellino, Design and simulation of a prototype
695 of a small-scale solar CHP system based on evacuated flat-plate solar collectors and Organic
696 Rankine Cycle, *Energy Convers. Manag.* 90 (2015) 347–363.
697 <https://doi.org/10.1016/j.enconman.2014.11.014>.
- 698 [13] T.C. Roumpedakis, G. Loumpardis, E. Monokrousou, K. Braimakis, A. Charalampidis, S.
699 Karellas, Exergetic and economic analysis of a solar driven small scale ORC, *Renew. Energy*.
700 157 (2020) 1008–1024. <https://doi.org/10.1016/j.renene.2020.05.016>.
- 701 [14] C. Kutlu, M.T. Erdinc, J. Li, Y. Wang, Y. Su, A study on heat storage sizing and flow control
702 for a domestic scale solar-powered organic Rankine cycle-vapour compression refrigeration
703 system, *Renew. Energy*. 143 (2019) 301–312. <https://doi.org/10.1016/j.renene.2019.05.017>.
- 704 [15] S. Quoilin, O. Dumont, K.H. Hansen, V. Lemort, Design, Modeling, and Performance
705 Optimization of a Reversible Heat Pump/Organic Rankine Cycle System for Domestic
706 Application, *J. Eng. Gas Turbines Power*. 138 (2016). <https://doi.org/10.1115/1.4031004>.
- 707 [16] Z. Liu, A. Romagnoli, P. Sapin, C. Markides, M. Mersch, Dynamic control strategies for a solar-
708 ORC system using first-law dynamic and data-driven machine learning models, (2021) 1–14.
- 709 [17] M. Ciani Bassetti, D. Consoli, G. Manente, A. Lazzaretto, Design and off-design models of a
710 hybrid geothermal-solar power plant enhanced by a thermal storage, *Renew. Energy*. 128 (2018)
711 460–472. <https://doi.org/10.1016/j.renene.2017.05.078>.
- 712 [18] J.L. Wang, L. Zhao, X.D. Wang, A comparative study of pure and zeotropic mixtures in low-
713 temperature solar Rankine cycle, *Appl. Energy*. 87 (2010) 3366–3373.
714 <https://doi.org/10.1016/j.apenergy.2010.05.016>.

- 715 [19] G. Qiu, Selection of working fluids for micro-CHP systems with ORC, *Renew. Energy*. 48
716 (2012) 565–570. <https://doi.org/10.1016/j.renene.2012.06.006>.
- 717 [20] R. Rayegan, Y.X. Tao, A procedure to select working fluids for Solar Organic Rankine Cycles
718 (ORCs), *Renew. Energy*. 36 (2011) 659–670. <https://doi.org/10.1016/j.renene.2010.07.010>.
- 719 [21] B.F. Tchanche, G. Papadakis, G. Lambrinos, A. Frangoudakis, Fluid selection for a low-
720 temperature solar organic Rankine cycle, *Appl. Therm. Eng.* 29 (2009) 2468–2476.
721 <https://doi.org/10.1016/j.applthermaleng.2008.12.025>.
- 722 [22] M. Bianchi, L. Branchini, A. De Pascale, F. Melino, S. Ottaviano, A. Peretto, N. Torricelli,
723 Performance modelling and greenhouse impact assessment of a micro-ORC energy system
724 working with HFCs, low GWP fluids and mixtures, in: *100RES 2020 – Appl. Energy Symp.*,
725 2020.
- 726 [23] K. Yadav, A. Sircar, Selection of working fluid for low enthalpy heat source Organic Rankine
727 Cycle in Dholera, Gujarat, India, *Case Stud. Therm. Eng.* 16 (2019) 100553.
728 <https://doi.org/10.1016/j.csite.2019.100553>.
- 729 [24] J. Bao, L. Zhao, A review of working fluid and expander selections for organic Rankine cycle,
730 *Renew. Sustain. Energy Rev.* 24 (2013) 325–342. <https://doi.org/10.1016/j.rser.2013.03.040>.
- 731 [25] I.H. Bell, P.A. Domanski, M.O. McLinden, G.T. Linteris, The hunt for nonflammable refrigerant
732 blends to replace R-134a, *Int. J. Refrig.* 104 (2019) 484–495.
733 <https://doi.org/10.1016/J.IJREFRIG.2019.05.035>.
- 734 [26] Y. Heredia-Aricapa, J.M. Belman-Flores, A. Mota-Babiloni, J. Serrano-Arellano, J.J. García-
735 Pabón, Overview of low GWP mixtures for the replacement of HFC refrigerants: R134a, R404A
736 and R410A, *Int. J. Refrig.* 111 (2020) 113–123.
737 <https://doi.org/10.1016/J.IJREFRIG.2019.11.012>.
- 738 [27] F. Molés, J. Navarro-Esbrí, B. Peris, A. Mota-Babiloni, C. Mateu-Royo, R1234yf and R1234ze
739 as alternatives to R134a in Organic Rankine Cycles for low temperature heat sources, in: *Energy*
740 *Procedia*, Elsevier Ltd, 2017: pp. 1192–1198. <https://doi.org/10.1016/j.egypro.2017.12.380>.
- 741 [28] M. A. Ancona, M. Bianchi, L. Branchini, A. De Pascale, F. Melino, S. Ottaviano, A. Peretto, N.
742 Torricelli, Performance prediction and design optimization of a kW-size reciprocating piston
743 expander working with low-GWP fluids, (2019).
- 744 [29] X.D. Wang, L. Zhao, Analysis of zeotropic mixtures used in low-temperature solar Rankine
745 cycles for power generation, *Sol. Energy*. 83 (2009) 605–613.
746 <https://doi.org/10.1016/j.solener.2008.10.006>.
- 747 [30] G. Bamorovat Abadi, E. Yun, K.C. Kim, Experimental study of a 1 kw organic Rankine cycle
748 with a zeotropic mixture of R245fa/R134a, *Energy*. 93 (2015) 2363–2373.
749 <https://doi.org/10.1016/j.energy.2015.10.092>.
- 750 [31] M. Bianchi, L. Branchini, A. De Pascale, F. Melino, S. Ottaviano, A. Peretto, N. Torricelli,
751 Replacement of R134a with low-GWP fluids in a kW-size reciprocating piston expander:
752 Performance prediction and design optimization, *Energy*. 206 (2020) 118174.
753 <https://doi.org/10.1016/j.energy.2020.118174>.
- 754 [32] M. Bianchi, L. Branchini, N. Casari, A. De Pascale, F. Melino, S. Ottaviano, M. Pinelli, P.R.
755 Spina, A. Suman, Experimental analysis of a micro-ORC driven by piston expander for low-
756 grade heat recovery, *Appl. Therm. Eng.* 148 (2019) 1278–1291.
757 <https://doi.org/10.1016/j.applthermaleng.2018.12.019>.
- 758 [33] R. Dickes, O. Dumont, R. Daccord, S. Quoilin, V. Lemort, Modelling of organic Rankine cycle
759 power systems in off-design conditions: An experimentally-validated comparative study,
760 *Energy*. 123 (2017) 710–727. <https://doi.org/10.1016/j.energy.2017.01.130>.
- 761 [34] PDR: NIST Reference Fluid Thermodynamic and Transport Properties Database (REFPROP)
762 Version 9 - SRD 23, (n.d.).
763 <https://data.nist.gov/od/id/ECBCC1C130222ED9E04306570681B10740> (accessed December 2,
764 2021).
- 765 [35] I. Garcia-Saez, J. Méndez, C. Ortiz, D. Loncar, J.A. Becerra, R. Chacartegui, Energy and
766 economic assessment of solar Organic Rankine Cycle for combined heat and power generation
767 in residential applications, *Renew. Energy*. 140 (2019) 461–476.
768 <https://doi.org/10.1016/j.renene.2019.03.033>.
- 769 [36] Residential Heating Residential Cooling Heat Pumps Solar Thermal and Cylinders Commercial

- 770 Heating Commercial Cooling System Complementary Items PRODUCT CATALOGUE 2015
771 INTERNATIONAL MARKETS, (2015). www.riello.com (accessed December 2, 2021).
- 772 [37] M. Bianchi, L. Branchini, A. De Pascale, F. Melino, S. Ottaviano, A. Peretto, N. Torricelli,
773 Application and comparison of semi-empirical models for performance prediction of a kW-size
774 reciprocating piston expander, *Appl. Energy*. 249 (2019) 143–156.
775 <https://doi.org/10.1016/j.apenergy.2019.04.070>.
- 776 [38] D. Ziviani, B.J. Woodland, E. Georges, E.A. Groll, J.E. Braun, W. Travis Horton, M. Van Den
777 Broek, M. De Paepe, Development and a Validation of a Charge Sensitive Organic Rankine
778 Cycle (ORC) Simulation Tool, (2015) 30. <https://doi.org/10.3390/en9060389>.
- 779 [39] R. Dickes, O. Dumont, L. Guillaume, S. Quoilin, V. Lemort, Charge-sensitive modelling of
780 organic Rankine cycle power systems for off-design performance simulation, *Appl. Energy*. 212
781 (2018) 1262–1281. <https://doi.org/10.1016/j.apenergy.2018.01.004>.
- 782 [40] D. Ziviani, R. Dickes, V. Lemort, J.E. Braun, E.A. Groll, Effects of the Working Fluid Charge
783 in Organic Rankine Cycle Power Systems: Numerical and Experimental Analyses, in: *Org. Rank.*
784 *Cycle Technol. Heat Recover., InTech*, 2018. <https://doi.org/10.5772/intechopen.78026>.
- 785 [41] A. Giuffrida, Modelling the performance of a scroll expander for small organic Rankine cycles
786 when changing the working fluid, *Appl. Therm. Eng.* 70 (2014) 1040–1049.
787 <https://doi.org/10.1016/j.applthermaleng.2014.06.004>.
- 788 [42] Global Warming Potential Values, (2021). www.ipcc.ch (accessed November 23, 2021).
- 789 [43] Y. Khan, R.S. Mishra, Performance analysis of solar driven combined recompression main
790 compressor intercooling supercritical CO₂ cycle and organic Rankine cycle using low GWP
791 fluids, *Energy Built Environ.* (2021) e00118. <https://doi.org/10.1016/J.ENBENV.2021.05.004>.
- 792 [44] UNI 10349 standards, (2016). <http://store.uni.com/catalogo/index.php/uni-10349-1-2016>.
- 793 [45] Panels inclination, (2010). <https://www.aggiustatutto.it/varie/nozioni-varie/353-inclinazione-pannelli-fotovoltaici-solari-termici.html>.
- 794
- 795 [46] Average daily monthly global solar radiation, on a horizontal surface, (2020).
796 <http://www.solaritaly.enea.it/CalcRgmmOrizz/Calcola.php>.
- 797 [47] P.S. Ennio Macchi, Stefano Campanari, La climatizzazione a gas e ad azionamento termico, n.d.
- 798 [48] Electricity prices in Italy, (2020). <https://www.qualenergia.it/articoli/come-vanno-i-prezzi-dellenergia-elettrica-in-italia-i-dati-dellautorita/>.
- 799
- 800 [49] Micro-ORC price, (2018). <https://airsquared.com/news/introducing-plug-play-micro-orc/>.
- 801 [50] Cambio Euro Dollaro 2021 Storico - cambioeuro, (n.d.). <https://www.cambioeuro.it/cambio-storico-dollaro-2021/>.
- 802
- 803 [51] S.A. Kalogirou, R. Agathokleous, G. Barone, A. Buonomano, C. Forzano, A. Palombo,
804 Development and validation of a new TRNSYS Type for thermosiphon flat-plate solar thermal
805 collectors: energy and economic optimization for hot water production in different climates,
806 *Renew. Energy*. 136 (2019) 632–644. <https://doi.org/10.1016/J.RENENE.2018.12.086>.
- 807 [52] M. Bianchi, L. Branchini, A. De Pascale, F. Melino, A. Peretto, D. Archetti, F. Campana, T.
808 Ferrari, N. Rossetti, Feasibility of ORC application in natural gas compressor stations, *Energy*.
809 173 (2019) 1–15. <https://doi.org/10.1016/J.ENERGY.2019.01.127>.
- 810